Phase Morphology of Ternary Mixtures under Shear

Gokul Raman Arumugam Kumar[2 [0009−0003−8901−0853]] and Ulf D. Schiller[1,2 [0000−0001−8941−1284]]

[1] Department of Computer and Information Sciences, University of Delaware, 101 Smith Hall, Newark, DE 19716, USA
[2] Department of Materials Science and Engineering, University of Delaware, 201 DuPont Hall, Newark, DE 19716, USA
{gokul,uschill}@udel.edu

Abstract. Emulsions of immiscible liquids can be used as templates for fabricating microstructure materials, including membranes and porous electrodes. Control over the domain size and morphology is desirable in these applications. In this work, we investigate the formation of ternary emulsions under an applied shear flow and characterize the emerging phase morphology. Using the lattice Boltzmann method, we simulate phase separation of a ternary fluid mixture that is sheared between two moving boundaries. At low shear rates, complex structures such as double emulsions and worm-like domains emerge. At high shear rates, the domains form aligned bands whose width depends on the shear rate, fluid properties and fluid composition. These findings demonstrate that shear can be used to control domain morphology in emulsions, thereby enabling the design of porous materials and aligned scaffolds for tissue engineering applications.

Keywords: emulsion templating · ternary fluid · lattice Boltzmann

1 Introduction

Emulsion templating is a versatile approach for the fabrication of porous materials [39] that have applications in filtration [40], energy storage [3], and the biomedical domain [32]. In the emulsion templating process, a matrix of droplets or a bicontinuous structure of one phase is introduced into a polymer solution of another phase, typically stabilized by a surfactant, thereby forming a complex emulsion that serves as a template. Subsequent processing steps such as heating or freeze-drying followed by vitrification convert the emulsion into a porous scaffolds. Processing conditions and external factors such as pH, temperature, or shear are found to affect the resulting structure of the template emulsion [23]. The underlying mechanism for forming an emulsion is phase separation, where the segregation of fluid domains facilitates the formation of microstructure morphologies [39]. Controlling the size and shape of fluid domains is desirable for applications, e.g., in tissue engineering [4] where specific structures are needed

ICCS Camera Ready Version 2026
To cite this paper please use the final published version:
DOI: 10.1007/978-3-032-29909-3_45

to achieve required properties. For instance, the scaffold needed to address volumetric skeletal muscle loss [8] must have a hierarchically organized cable or band-like structure.

Shear in immiscible fluid mixtures [15,14] and emulsions [12] has been an active area of research in the past few decades and provides a means to to control the geometrical characteristics of fluid domains. Hashimoto et al. [15,14] investigated a binary fluid under varying shear rates to study the influence of shear on the steady-state morphology. Complementary computational studies have been employed by Chueh et al. [9] to characterize the phase separation kinetics and resulting morphologies over a range of shear rates and capillary numbers. Both studies found that band-like structures emerge at higher shear rates and provide detailed analyses of the associated kinetic processes. While binary fluid systems have been extensively studied in both quiescent conditions and under shear, ternary fluid systems remain comparatively underexplored. In the quiescent state, phase separation of ternary fluids and the emerging morphologies have been studied by Semprebon et al.[28], and Kusumaatmaja et al.[31]. These works showed that the presence of a third component can give rise to more complex structures than those observed in binary systems. One such example is the caterpillar-like morphology formed by adjacent droplets of two fluid components within a continuous third component. Few investigations of ternary fluid systems under shear are currently available, including the work by Travesso et al. [37] who studied the effect of shear on a homogeneous ternary mixture and used the findings as input to a lattice-spring model to characterize the system's micromechanics. However, they considered only one fixed set of fluid properties and focused on the mechanical properties of the resulting emulsion rather than on the effect of fluid properties on the emulsion morphology.

Since experiments provide limited insight into both kinetic processes and final domain morphologies, computational approaches are useful to investigate liquid emulsions. A variety of computational techniques are available to simulate multicomponent fluids, including Molecular Dynamics [21], Monte Carlo [27], Dissipative Particle Dynamics [34], Finite Difference and Finite Element Methods [10,24], and Lattice Boltzmann Methods [29,30,36,35,26,13,38]. The lattice Boltzmann method (LBM) is particularly suited to study complex emulsions owing to its ability to handle complex boundary conditions and its embarrassingly parallel nature, which facilitates large-scale simulations on parallel computing systems. The lattice Boltzmann method reproduces the macroscopic hydrodynamic equations of incompressible liquids, including the Navier-Stokes equation [11,19]. Several extensions of the LBM enable simulations of multiphase and multicomponent fluids, e.g., the Shan-Chen model [29,30], the Color-Gradient model [26,13], and the free-energy model [36,35].

In this work, we employ the lattice Boltzmann method for ternary fluids [28] to investigate the domain morphology of ternary mixtures undergoing phase separation in a shear flow. We characterize the effects of fluid properties, composition, and shear rate on the steady-state final morphology. Our results reveal the general layout of the morphology for different shear rates: double emulsions form

ICCS Camera Ready Version 2026
To cite this paper please use the final published version:
DOI: 10.1007/978-3-032-29909-3_45

at lower shear rates, while band-like domains form at higher shear rates. The thickness of the band-like domains depends on fluid properties, composition and shear rate. Our findings highlight the effects that govern phase separation and shear, as well as the added complexity introduced by the third component. The results provide quantitative insights that can be leveraged in creating emulsion templates for fabrication of soft materials with tailored structure and properties.

2 Methods

2.1 Equations of Motion of a Ternary Fluid

We consider a fluid mixture consisting of three components C_i. The thermodynamics of the mixture is specified in terms of a free energy F. A common choice for immiscible fluids is a double-well free energy of the form [6,28]

$$\frac{F}{\rho k_B T} = \int_V \left[\sum_{i=1}^{3} \frac{\lambda_i}{2} C_i^2 (1 - C_i)^2 + \frac{\kappa_i}{2} (\nabla C_i)^2 \right] dV, \tag{1}$$

where C_i is the mass composition of the ternary fluid mixture. The square gradient terms $(\nabla C)^2$ introduce an energy cost for interfaces that gives rise to interfacial tension [7]. The interfacial tension between components m and n is given by [28]

$$\sigma_{mn} = \frac{1}{6} \sqrt{(\lambda_m + \lambda_n)(\kappa_m + \kappa_n)}. \tag{2}$$

In thermodynamic equilibrium, the stationary solution of the free energy yields a diffuse interface profile with an interface width proportional to

$$\alpha = \sqrt{\frac{\kappa_m + \kappa_n}{\lambda_m + \lambda_n}}. \tag{3}$$

In the remainder of this paper, we will set $\kappa_i = \alpha^2 \lambda_i$ for all components such that the interfacial tension is

$$\sigma_{mn} = \frac{1}{6\alpha} (\kappa_m + \kappa_n). \tag{4}$$

The fluid motion of the mixture is governed by the Cahn-Hilliard-Navier-Stokes equations [17]

$$\frac{\partial \rho}{\partial t} + \nabla \cdot (\rho \vec{u}) = 0, \tag{5}$$

$$\begin{aligned} \frac{\partial (\rho \vec{u})}{\partial t} + \nabla \cdot (\rho \vec{u} \vec{u}) = &-\nabla p_{\mathrm{id}} + \nabla \cdot \eta (\nabla \vec{u} + \nabla \vec{u}^{\mathrm{T}}) \\ &- \rho \nabla \mu_\rho - \phi \nabla \mu_\phi - \psi \nabla \mu_\psi, \end{aligned} \tag{6}$$

$$\frac{\partial \phi}{\partial t} + \nabla \cdot (\phi \vec{u}) = M_\phi \nabla^2 \mu_\phi, \tag{7}$$

$$\frac{\partial \psi}{\partial t} + \nabla \cdot (\psi \vec{u}) = M_\psi \nabla^2 \mu_\psi, \tag{8}$$

ICCS Camera Ready Version 2026
To cite this paper please use the final published version:
DOI: 10.1007/978-3-032-29909-3_45

where η is the dynamic viscosity, and M_ϕ and M_ψ are mobility parameters. In the LBM, the isotropic pressure p is the ideal gas pressure $p = \rho c_s^2$, where c_s denotes the lattice speed of sound (see below). In the equations of motion, we have introduced the density ρ and scalar order parameters ϕ and ψ

$$\rho = C_1 + C_2 + C_3, \qquad \phi = C_1 - C_2, \qquad \psi = C_3. \tag{9}$$

The chemical potentials corresponding to the fields ρ, ϕ, and ψ are obtained by rewriting the free energy in the appropriate variables and taking variational derivatives

$$\mu_\rho = \frac{\delta F}{\delta \rho}, \qquad \mu_\phi = \frac{\delta F}{\delta \phi}, \qquad \mu_\psi = \frac{\delta F}{\delta \psi}. \tag{10}$$

The gradients of the chemical potential are the driving forces that give rise to phase segregation and diffusion.

2.2 Lattice Boltzmann Method

The lattice Boltzmann method (LBM) is a discrete kinetic model of the Boltzmann equation. In the discrete formulation, the basic variables are distribution functions $f_i(\vec{x}, t)$, also referred to as populations. $f_i(\vec{x}, t)$ represents the fluid mass density at a discrete lattice position x at time t that moves along a discrete velocity vector $\vec{c_i}$. The discrete velocities $\vec{c_i}$ connect the nodes of a regular cubic lattice. In this work, we use the $D3Q19$ velocity set which includes a zero velocity and the velocity vectors that connect the six nearest and twelve next-nearest neighbors on a 3D lattice.

To model a multicomponent fluid, multiple distribution functions are used. For a ternary mixture, we choose three distribution functions f_i, g_i, and h_i corresponding to the scalar fields ρ, ϕ, and ψ. The macroscopic variables are obtained as moments of the distribution functions

$$\rho = \sum_i f_i, \qquad \phi = \sum_i g_i, \qquad \psi = \sum_i h_i, \tag{11}$$

and the bulk flow velocity $\vec{u}$ of the mixture is given in terms of the first moment of f_i

$$\rho \vec{u} = \sum_i f_i \vec{c}_i. \tag{12}$$

The discrete-time evolution of the distribution functions is described by the lattice Boltzmann equations

$$f_i(\vec{x} + \Delta t \vec{c_i}, t + \Delta t) = f_i^*(\vec{x}, t) = f_i(\vec{x}, t) - \frac{\Delta t}{\tau_\rho} \left[f_i(\vec{x}, t) - f_i^{\mathrm{eq}}(\vec{x}, t) \right], \tag{13}$$

$$g_i(\vec{x} + \Delta t \vec{c_i}, t + \Delta t) = g_i^*(\vec{x}, t) = g_i(\vec{x}, t) - \frac{\Delta t}{\tau_\phi} \left[g_i(\vec{x}, t) - g_i^{\mathrm{eq}}(\vec{x}, t) \right], \tag{14}$$

$$h_i(\vec{x} + \Delta t \vec{c_i}, t + \Delta t) = h_i^*(\vec{x}, t) = h_i(\vec{x}, t) - \frac{\Delta t}{\tau_\psi} \left[h_i(\vec{x}, t) - h_i^{\mathrm{eq}}(\vec{x}, t) \right], \tag{15}$$

ICCS Camera Ready Version 2026
To cite this paper please use the final published version:
DOI: 10.1007/978-3-032-29909-3_45

where Δt is the discrete time step, and we have used a standard Bhatnagar-Gross-Krook (BGK) collision approach [5] with a single relaxation time τ_ρ, τ_ϕ, and τ_ψ for each component, respectively. The equilibrium distribution functions f_i^{eq}, g_i^{eq}, and h_i^{eq} are constructed such that the correct form of the Cahn-Hilliard-Navier-Stokes equations is recovered within a second-order Chapman-Enskog expansion [20,25].

In the continuum limit, the ternary LBM then recovers the thermodynamic and hydrodynamic behavior of the Cahn-Hilliard-Navier-Stokes equations. The macroscopic transport coefficients are related to the relaxation times by the following expressions

$$\eta = \rho c_s^2 \left(\tau_\rho - \frac{\Delta t}{2}\right), \qquad M_\phi = \Gamma_\phi \left(\tau_\phi - \frac{\Delta t}{2}\right), \qquad M_\psi = \Gamma_\phi \left(\tau_\psi - \frac{\Delta t}{2}\right), \tag{16}$$

where Γ_ϕ and Γ_ψ are scalar parameters, and $c_s^2 = 1/3$ is the lattice speed of sound of the D3Q19 velocity set.

In this work, we leverage the implementation of the ternary free energy LBM in LAMMPS; for details, including explicit expressions for the equilibrium distribution functions f^{eq}, g^{eq}, and h^{eq} and the full expression for the thermodynamic pressure tensor, we refer the reader to Ref. [28,2].

2.3 Boundary Conditions

A linear shear flow can be applied to the fluid by imposing moving walls at the boundaries of the lattice. The velocity of the wall enters the moving bounce-back boundary condition [16] that replaces the periodic boundary condition on the first and last lattice layer

$$f_i(\vec{x} + \Delta t\vec{c_i}, t + \Delta t) = f_i^*(\vec{x}, t) - 2w_i\Delta t\frac{\vec{c_i}\cdot\vec{u_B}}{c_s^2}, \tag{17}$$

$$g_i(\vec{x} + \Delta t\vec{c_i}, t + \Delta t) = g_i^*(\vec{x}, t) - 2w_i\Delta t\frac{\vec{c_i}\cdot\vec{u_B}}{c_s^2}, \tag{18}$$

$$h_i(\vec{x} + \Delta t\vec{c_i}, t + \Delta t) = h_i^*(\vec{x}, t) - 2w_i\Delta t\frac{\vec{c_i}\cdot\vec{u_B}}{c_s^2}. \tag{19}$$

Here, $\vec{u}_B$ denotes the velocity of the boundary, and f_I^*, g_i^*, and h_i^* are post-collisional distributions, and w_i are the weight factors of the D3Q19 velocity set. The moving bounce-back condition is applied at the boundary planes at the two ends of the z-direction, while periodic boundary conditions are maintained in the other directions.

2.4 Simulation Setup and Dimensionless Parameters

For a multicomponent system undergoing phase separation in applied shear flow, multiple physical mechanisms are at play, the relative importance of which can be characterized using dimensionless parameters. The dynamics of the ternary

ICCS Camera Ready Version 2026
To cite this paper please use the final published version:
DOI: 10.1007/978-3-032-29909-3_45

mixture is controlled by the bulk fluid properties ρ and η, the transport coefficients M_ϕ, and M_ψ, and the three interfacial tensions σ_{12}, σ_{23}, σ_{31}. We will use the surface tension σ_{12} as the primary parameter and express the other two tensions by the following dimensionless ratios

$$r_\sigma = \frac{2\sigma_{12}}{\sigma_{23}+\sigma_{31}}, \qquad \Delta\sigma = \frac{\sigma_{31}-\sigma_{23}}{\sigma_{12}}. \tag{20}$$

Using the interface width α and shear velocity u_B to fix the length and time scale, we obtain four dimensionless parameters, the Reynolds number, the capillary number, and two Peclet numbers

$$\mathrm{Re} = \frac{\rho u_B \alpha}{\eta}, \qquad \mathrm{Ca} = \frac{\eta u_B}{\sigma_{12}}, \qquad \mathrm{Pe}_\phi = \frac{u_B \alpha^2}{M_\phi \sigma_{12}}, \qquad \mathrm{Pe}_\psi = \frac{u_B \alpha^2}{M_\psi \sigma_{12}}. \tag{21}$$

For our purposes, it will be convenient to consider the ratio of the Peclet number Pe_ϕ and the capillary number Ca, which is referred to as the fluidity parameter [9]

$$\mathrm{Flu} = \frac{\alpha^2}{\eta M_\phi}. \tag{22}$$

It can be conceived as the dimensionless number that governs the transport of the phase field ϕ

$$\frac{\partial \phi}{\partial \hat{t}} + \mathrm{Flu}\,\hat{\nabla}\cdot(\phi\hat{u}) = \hat{\nabla}^2\hat{\mu}_\phi, \tag{23}$$

where the chemical potential $\mu_\phi = (\sigma/\alpha)\hat{\mu}_\phi$ has been scaled with the interfacial energy, the velocity $\vec{u} = (\sigma/\eta)\hat{u}$ with the capillary velocity, and the time $t = \tau_D \hat{t}$ with the diffusion time $\tau_D = \alpha^3/(\sigma M_\phi)$. The fluidity parameter thus indicates whether mass transport is dominated by advection ($\mathrm{Flu} \gg 1$) or by diffusion ($\mathrm{Flu} \ll 1$). It only depends on intrinsic fluid properties and not the imposed shear rate γ.

In our simulation setup, we keep the following quantities constant: the density $\rho = 1\,\Delta m \Delta x^{-3}$, the viscosity $\eta = 1/6\,\Delta m \Delta x^{-1} \Delta t^{-1}$, and we set the interfacial tension ratios to $r_\sigma = 1$ and $\Delta\sigma = 0$ with $\alpha = 0.5\,\Delta x$. The LB relaxation times are kept fixed at unity $\tau_\rho = \tau_\phi = \tau_\psi = \Delta t$, and we chose the parameters Γ_ϕ and Γ_ψ to fix the mobility $M_\psi = 1/2\,\Delta m^{-1} \Delta x^3 \Delta t$, $M_\phi = 6\,\Delta m^{-1} \Delta x^3 \Delta t$ and thus fixing $Pe_\phi/Pe_\psi = 1/12$. Our choice of Pe_ϕ/Pe_ψ makes the kinetic transport of components 1 and 2 faster than that of component 3, exactly by a factor of 4 as $M_1 = M_2 = M_\phi/2$ and $M_3 = 3M_\psi/2$ [28]. The range of applied shear velocities u_B is chosen such that the Reynolds number remains negligibly small (≈ 0). The remaining parameters are used to vary the fluidity parameter Flu and the capillary number Ca to investigate the effects of fluid properties and shear rate on phase separation dynamics.

We performed lattice Boltzmann simulations of a ternary mixture on a quasi-2D lattice with dimension $l_x = 400\,\Delta x$, $l_y = 6\,\Delta x$, and $l_z = 200\,\Delta x$. The mixture is initialized with a homogeneous composition (C_1, C_2, C_3) with a small random perturbation to induce phase separation. A shear flow is generated by imposing

ICCS Camera Ready Version 2026
To cite this paper please use the final published version:
DOI: 10.1007/978-3-032-29909-3_45

equal and opposite velocities $\pm u_B$ along the x-axis at boundary planes located at the two ends of the z-direction. The simulations were run for a total time of $t_f = 2.4 \cdot 10^5\, \tau_D$. The snapshots were taken every $1200\tau_D$ timestep, ensuring that the initial coarsening dynamics are captured. Both the shear and phase separation start from $t = 0\tau_D$, i.e., the competing forces act from the beginning. For the rest of the paper, we refer to the applied shear through the dimensionless shear rate $\bar{\gamma} = \gamma \cdot \tau_D$, where $\gamma = 2u_B/l_z$.

3 Results and Discussion

3.1 Effect of Fluid Composition

Under quiescent conditions, spinodal decomposition of ternary mixtures can lead to various domain morphologies depending on the composition of the mixture. Ternary mixtures with homogeneous symmetric composition ($C_1 = C_2 = C_3$) results into foam-like morphologies, while mixtures with one dominant component (say $C_1 > C_2, C_3$) can form worm-like structure consisting of components 2 and 3 [28,2]. In this section, we investigate ternary phase separation in shear flow to probe the emerging morphologies for varying mixture composition. In the simulations, we fix the intrinsic fluid properties at Flu = 0.25 and impose a dimensionless shear rate of $\bar{\gamma} = 1.5625 \cdot 10^{-3}$. We compare two different mixture compositions: symmetric composition $C_1 = C_2 = C_3$, and asymmetric composition $C_1 = 0.5$, $C_2 = 0.3$, $C_3 = 0.2$.

Snapshots of the domain morphology at the end of the simulation runs are shown in Fig. 1. At symmetric composition, we observe the formation of elongated band-like domains of all three components in the center of the channel, while some worm-like structures emerge at the bounding walls. The formation of these structures is facilitated by the neutral contact angle of the interface between any two components and the wall. For the asymmetric composition, we observe band-like structures for the two dominant components 1 and 2, while the minority component 3 forms both stretched liquid-lenses at the interface between 1 and 2 and partially wetting droplets at the wall.

In the symmetric composition mixture, all three components form bands; in the asymmetric composition case, only the two majority components form bands. We find by visual inspection that the width of the bands of the symmetric composition mixture is about 40% smaller than in the asymmetric composition. This is most likely due to hindrance of coalescence: once a percolating band has formed in the system, it effectively acts as a barrier to domain growth perpendicular to the flow direction. Hence, while band-like structures are observed in both cases, the composition determines the specific types and sizes of bands that can form. In the following, we investigate whether the emulsion structure can be further tuned by varying the applied shear rate.

3.2 Effect of Shear Rate

To study the effect of the shear rate on the phase separation dynamics, we fixed the fluid composition at $C_1 = 0.5, C_2 = 0.3, C_3 = 0.2$, and chose the fluid

ICCS Camera Ready Version 2026
To cite this paper please use the final published version:
DOI: 10.1007/978-3-032-29909-3_45

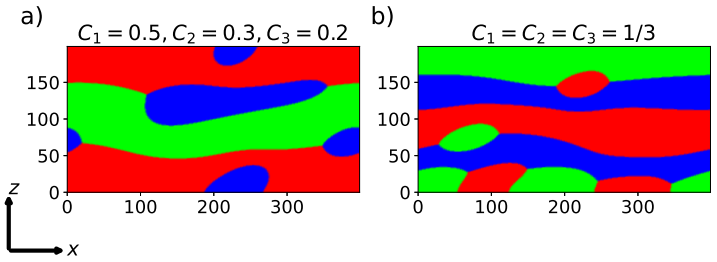

Fig. 1. Band-like Morphology of (a) $C_1 = 0.5, C_2 = 0.3, C_3 = 0.2$, (b) $C_1 = C_2 = C_3 = 1/3$, at Flu $= 0.25$ and $\bar{\gamma} = 1.5625 \cdot 10^{-3}$. The morphology is shown at $t = 2.4 \cdot 10^5 \tau_D$. The red, green, and blue colors represent components 1, 2, and 3.

properties such that Flu $= 0.25$. We ran a set of simulations with varying shear velocity corresponding to the capillary and Peclet numbers shown in Table 1.

Snapshots of the final domain morphology are shown in Fig. 2. Two distinct types of emulsions can be observed: at low shear rate ($\bar{\gamma} = 6.25{\cdot}10^{-5},\ 3.125{\cdot}10^{-4}$) double emulsion structures alternating in component 2 and 3 surrounded by the majority component 1. At higher rates ($\bar{\gamma} = 1.5625{\cdot}10^{-3},\ 3.125{\cdot}10^{-3}$), band-like structures of component 1 and component 2 extend along the flow direction in the surrounding component 1. The formation of worm-like double emulsions at lower shear rates is facilitated by migration and partial coalescence of domains of the minority components [1]. At higher shear rates, the viscous forces begin to dominate and stretch segregated domains into the band-like structures [15,14].

To characterize the phase separation dynamics quantitatively, we investigate the time evolution of the average domain size of component 2. We chose component 2 because the intermediate-concentration component develops well-defined domains over the course of the simulation. We use the mean intercept length to measure the average domain size [33,22]. To compute the mean intercept length, the following steps are taken: (1) draw a family of parallel lines, parallel to a specified direction v, (2) count the number of intersections, I_v, between these

Table 1. Wall velocities applied to generate varying shear rates. The table indicates the value of the shear velocity u_B, the dimensionless shear rate $\bar{\gamma} = \gamma{\cdot}\tau_D$, the corresponding capillary number Ca, and Peclet Number Pe_ϕ. The intrinsic fluid properties are kept constant such that Flu $= 0.25$.

$u_B \cdot \Delta t/\Delta x$	$\bar{\gamma} = 2u_B/l_z \cdot \tau_D$	Ca	Pe_ϕ	Flu
0.0005	$6.25 \cdot 10^{-5}$	0.05	0.0125	0.25
0.0025	$3.125 \cdot 10^{-4}$	0.25	0.0625	0.25
0.0125	$1.5625 \cdot 10^{-3}$	1.25	0.3125	0.25
0.025	$3.125 \cdot 10^{-3}$	2.5	0.625	0.25

ICCS Camera Ready Version 2026
To cite this paper please use the final published version:
DOI: 10.1007/978-3-032-29909-3_45

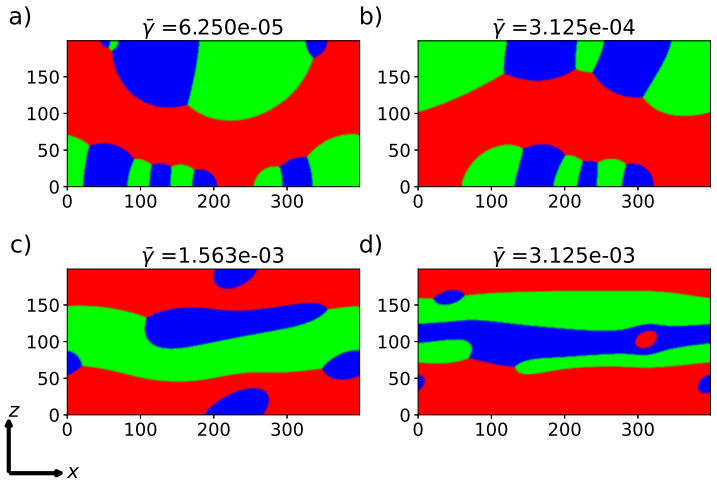

Fig. 2. Morphology of a ternary mixture with composition $C_1 = 0.5, C_2 = 0.3, C_3 = 0.2$ and fluidity parameter Flu $= 0.25$ for varying shear rates $\bar{\gamma}$. Qualitative change in the class of morphology can be observed. Lower shear rates (a, b) produce double emulsion and worm-like morphology, while higher shear rates (c, d) result in band-like structure. The snapshots show the emulsion morphology at $t = 2.4 \cdot 10^5\, \tau_D$. The red, green, and blue colors represent components 1, 2, and 3, respectively.

lines and the Component 2 phase, (3) compute the mean intercept length (L_v) measured along the direction v through the equation below,

$$L_v = \frac{h}{I_v} \tag{24}$$

where h represents the summation of all the lengths drawn. Here, we measure the mean intercept length along the x- and z-directions, denoted by L_x and L_z, respectively.

The time evolution of the domain sizes in these directions is shown in Fig. 3 for the lower shear rates, and in Fig. 4 for the higher shear rates. We find that at lower shear rates (Fig. 3), the evolution of the domain size is well described by a power law with a growth exponent of 1/3. This is the typical Ostwald ripening growth law, and it is consistent with the observed domain growth in both directions parallel and perpendicular to the shear flow. This indicates that at low shear rates, the phase separation kinetics are not significantly altered compared to the quiescent case and remain isotropic.

At higher shear rates (Fig. 4), we find that the coarsening kinetics depend on direction. In the direction parallel to the shear flow, the growth of L_x is well described by a power law with an exponent of 1. This exponent indicates that the domain growth corresponds to the viscous regime [18], where capillary forces

ICCS Camera Ready Version 2026
To cite this paper please use the final published version:
DOI: 10.1007/978-3-032-29909-3_45

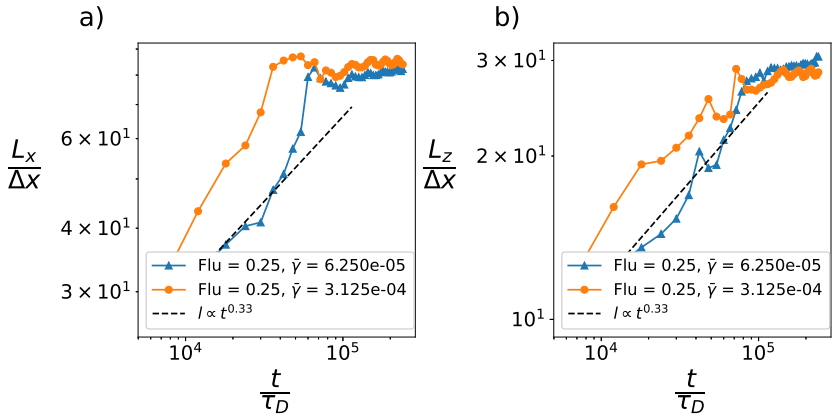

Fig. 3. Time evolution of domain size for shear rates $\bar{\gamma} = 6.25 \cdot 10^{-5}, 3.125 \cdot 10^{-4}$. (a) Domain size L_x along the x-direction. (b) Domain size L_z along the z-direction. Both L_x and L_z follow a power law with a growth exponent of 1/3, indicative of an isotropic diffusive domain growth.

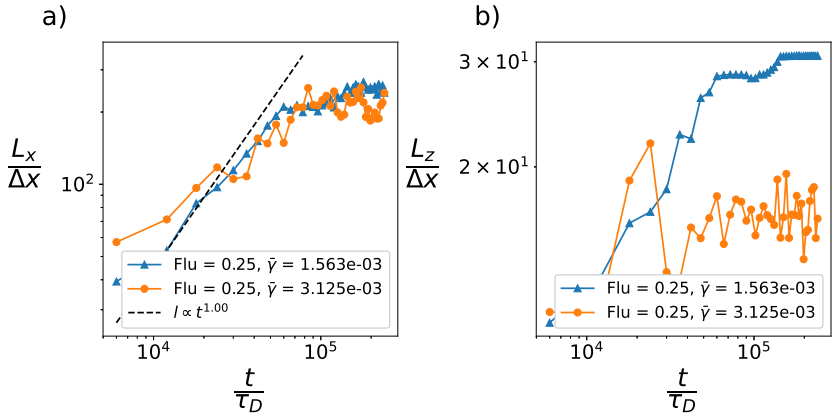

Fig. 4. Time evolution of domain size for shear rates $\bar{\gamma} = 1.5625 \cdot 10^{-3}, 3.125 \cdot 10^{-3}$. (a) Domain size L_x along the x-direction. (b) Domain size L_z along the z-direction. L_x follows a power law with a growth exponent of 1, indicative of the viscous coarsening regime.

ICCS Camera Ready Version 2026
To cite this paper please use the final published version:
DOI: 10.1007/978-3-032-29909-3_45

are balanced by viscous forces such that Ca ~ 1 and $L \sim \sigma/\eta\, t$. In the direction perpendicular to the walls, the evolution of L_z is characterized by the formation of band-like structures. The average thickness of the band-like structures depends on the shear rate, and Fig. 4b suggests that the band thickness decreases with increasing shear rate. The shear rate is thus one possible factor to control the morphology of ternary emulsion templates.

3.3 Effect of Intrinsic Fluid Properties

Having shown that ternary phase separation in shear flow can lead to a band-like emulsion structure, we investigate the dependence of this effect on the intrinsic fluid properties. In particular, we study how the fluid viscosity and the interfacial tension affect the formation of elongated, anisotropic domains. For the simulations in this section, we fix the fluid composition at $C_1 = 0.5, C_2 = 0.3, C_3 = 0.2$ and impose a fixed dimensionless shear rate of $\bar{\gamma} = 1.5625 \cdot 10^{-3}$. This shear rate produces band-like structures at a fluidity parameter Flu $= 0.25$. The definition (22) of the fluidity parameter can be rewritten in terms of the dimensionless shear rate

$$\mathrm{Flu} = \frac{l_z}{2\alpha}\frac{\bar{\gamma}}{\mathrm{Ca}} = \frac{l_z}{2\alpha}\frac{\bar{\gamma}\sigma_{12}}{\eta u_B}. \tag{25}$$

Here, we vary the fluidity parameter by adjusting σ_{12} and M_ϕ such that $\mathrm{Pe}_\phi = \bar{\gamma} l_z/(2\alpha)$ remains constant. We ran simulations at two different values of the fluidity parameter corresponding to the parameters shown in Table 2

Snapshots of the domain morphology at the end of the simulation are shown in Fig. 5. Band-like structures similar to those observed in section 3.1 develop at both values of the fluidity parameter. At lower fluidity parameter, a larger number of bands is observed, and the width of the bands is smaller. At the higher fluidity number, only a single band of component 1 and 2 is observed, whose width is accordingly larger. These observations are consistent with the interpretation of the fluidity parameter as an inverse capillary number. Since we keep the Peclet number Pe_ϕ (a multiple of the dimensionless shear rate) fixed, a larger fluidity parameter corresponds to a higher surface tension, i.e., a lower capillary number. At lower capillary number, the energy penalty of forming interfaces is larger, and thus coarsening of thinner bands into fewer wider bands is favorable. In addition, the typical capillary-induced velocity increases which may drive coalescence. These findings suggest that the intrinsic fluid properties such as the surface tension can be linked to the domain morphology, specifically, the width of band-like structures that emerge at higher shear rates. In practice,

Table 2. Tabulation indicating the choice of κ ($\kappa_1 = \kappa_2 = \kappa_3 = \kappa$) and M_ϕ used to vary Flu and Ca, while fixing $\mathrm{Pe}_\phi = 0.3125$.

$\kappa \cdot \Delta m^{-1}\Delta x \Delta t^2$	$\sigma_{12} \cdot \Delta m^{-1}\Delta t^2$	$M_\phi \cdot \Delta m \Delta x^{-3}\Delta t^{-1}$	Ca	Pe_ϕ	Flu
$2.5 \cdot 10^{-4}$	$1.67 \cdot 10^{-4}$	60	12.5	0.3125	0.025
$2.5 \cdot 10^{-3}$	$1.67 \cdot 10^{-3}$	6	1.25	0.3125	0.25

ICCS Camera Ready Version 2026
To cite this paper please use the final published version:
DOI: 10.1007/978-3-032-29909-3_45

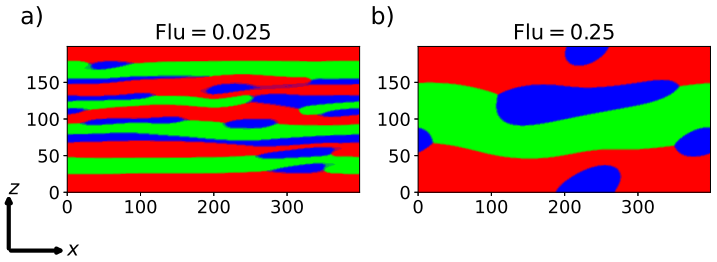

Fig. 5. Band-like morphology of $C_1 = 0.5, C_2 = 0.3, C_3 = 0.2$ and $\bar{\gamma} = 1.5625 \cdot 10^{-3}$ at (a) Flu = 0.025, and (b)Flu = 0.25. The morphology is shown at $t = 2.4 \cdot 10^5 \tau_D$. The red, green, and blue colors represent components 1, 2, and 3.

there may be stimuli-responsive mechanisms (e.g., temperature or pH) to tune the fluid properties that will allow to tailor the formation of band-like domains.

4 Conclusion

We have performed lattice Boltzmann simulations of phase separation of ternary mixtures in an applied shear flow. The study was motivated by applications of emulsions as templates for fabrication of porous materials. Our results show that shear flow can elongate fluid domains and lead to a band-like morphology. The precise morphology is dependent on various parameters including the fluid composition, the intrinsic fluid properties, and the shear rate. A sufficiently high shear rate is required to observe percolating domains that form bands, and the width of the bands is further controlled by the competition of capillary, viscous, and diffusive transport. We have used the fluidity parameter, i.e., the ratio of the Peclet and the capillary number to characterize the intrinsic fluid properties. Our results also reveal the kinetics of phase separation under shear: at lower shear rates, the domain coarsening follows a power law with a growth exponent 1/3 indicative of Ostwald ripening. At higher shear rates, the coarsening kinetics exhibits a power-law exponent of 1, indicative of the viscous regime. Moreover, higher shear rates induce the formation of the elongated domains that may percolate to form band-like emulsion morphologies.

The emulsion morphologies observed in our simulations are likely not exhaustive. Other material properties and parameters, such as contact angles, concentration-dependent fluid properties, or time-dependent shear flows, are potential alternative ways to modulate phase separation kinetics and domain morphology. Furthermore, we used a pseudo-2D simulation domain, and while we expect the qualitative effects of shear to be unchanged (especially for high shear rates), studying the morphology of emulsions in a fully 3D simulation domain would be of interest in future investigations.

ICCS Camera Ready Version 2026
To cite this paper please use the final published version:
DOI: 10.1007/978-3-032-29909-3_45

The results presented in this work highlight the interplay of capillary, viscous, and diffusion effects in phase separation under shear, and the insights drawn from the simulations can support the design and fabrication of emulsion templates for porous materials, tissue engineering, and other applications.

Acknowledgments. This work was supported by the National Science Foundation under NSF Awards DMR-2414458 and OIA-2346036. Any opinions, findings and conclusions or recommendations expressed in this material are those of the authors and do not necessarily reflect those of the National Science Foundation. This research was supported in part through the use of DARWIN computing system: DARWIN – A Resource for Computational and Data-intensive Research at the University of Delaware and in the Delaware Region, Rudolf Eigenmann, Benjamin E. Bagozzi, Arthi Jayaraman, William Totten, and Cathy H. Wu, University of Delaware, 2021, https://udspace.udel.edu/handle/19716/29071.

Disclosure of Interests. The authors have no competing interests.

References

1. Al-Mulla, A., Gupta, R.K.: Droplet coalescence in the shear flow of model emulsions. Rheologica Acta **39**(1), 20–25 (Jan 2000). https://doi.org/10.1007/s003970050003
2. Arumugam Kumar, G.R., Andrews, J.P., Schiller, U.D.: Implementation of a ternary lattice Boltzmann model in LAMMPS. Computer Physics Communications **294**, 108898 (Jan 2024). https://doi.org/10.1016/j.cpc.2023.108898
3. Asfaw, H.D., Roberts, M., Younesi, R., Edstrom, K.: Emulsion-templated bicontinuous carbon network electrodes for use in 3D microstructured batteries. Journal of Materials Chemistry A **1**(44), 13750 (2013). https://doi.org/10.1039/c3ta12680c
4. Ben Messaoud, G., Stefanopoulou, E., Wachendörfer, M., Aveic, S., Fischer, H., Richtering, W.: Structuring gelatin methacryloyl – dextran hydrogels and microgels under shear. Soft Matter **20**(4), 773–787 (2024). https://doi.org/10.1039/D3SM01365K
5. Bhatnagar, P.L., Gross, E.P., Krook, M.: A Model for Collision Processes in Gases. I. Small Amplitude Processes in Charged and Neutral One-Component Systems. Physical Review **94**(3), 511–525 (May 1954). https://doi.org/10.1103/PhysRev.94.511
6. Boyer, F., Lapuerta, C.: Study of a three component Cahn-Hilliard flow model. ESAIM: Mathematical Modelling and Numerical Analysis **40**(4), 653–687 (Jul 2006). https://doi.org/10.1051/m2an:2006028
7. Cahn, J.W., Hilliard, J.E.: Free Energy of a Nonuniform System. I. Interfacial Free Energy. The Journal of Chemical Physics **28**(2), 258–267 (1958). https://doi.org/10.1063/1.1744102
8. Carnes, M.E., Pins, G.D.: Skeletal Muscle Tissue Engineering: Biomaterials-Based Strategies for the Treatment of Volumetric Muscle Loss. Bioengineering **7**(3), 85 (Jul 2020). https://doi.org/10.3390/bioengineering7030085
9. Chueh, C.C., Bertei, A., Mauri, R.: Dynamics of phase separation of sheared inertialess binary mixtures. Physics of Fluids **32**(2), 023307 (Feb 2020). https://doi.org/10.1063/1.5144404

ICCS Camera Ready Version 2026
To cite this paper please use the final published version:
DOI: 10.1007/978-3-032-29909-3_45

10. Donev, A., Nonaka, A., Bhattacharjee, A.K., Garcia, A.L., Bell, J.B.: Low Mach number fluctuating hydrodynamics of multispecies liquid mixtures. Physics of Fluids **27**(3), 037103 (2015). https://doi.org/10.1063/1.4913571
11. Dünweg, B., Schiller, U.D., Ladd, A.J.C.: Statistical mechanics of the fluctuating lattice Boltzmann equation. Physical Review E **76**(3), 036704 (2007). https://doi.org/10.1103/PhysRevE.76.036704
12. Foudazi, R., Zhao, B., Gokun, P., Manas-Zloczower, I., Rowan, S.J., Feke, D.L.: The Effect of Shear on the Evolution of Morphology in High Internal Phase Emulsions Used as Templates for Structural and Functional Polymer Foams. ACS Applied Polymer Materials **2**(4), 1579–1586 (2020). https://doi.org/10.1021/acsapm.0c00003
13. Grunau, D., Chen, S., Eggert, K.: A lattice Boltzmann model for multiphase fluid flows. Physics of Fluids A: Fluid Dynamics **5**(10), 2557–2562 (1993). https://doi.org/10.1063/1.858769
14. Hashimoto, T., Matsuzaka, K., Moses, E., Onuki, A.: String Phase in Phase-Separating Fluids under Shear Flow. Physical Review Letters **74**(1), 126–129 (Jan 1995). https://doi.org/10.1103/PhysRevLett.74.126
15. Hashimoto, T., Takebe, T., Suehiro, S.: Ordered structure and critical phenomena of a semidilute solution of polymer mixtures under shear flow. The Journal of Chemical Physics **88**(9), 5874–5881 (May 1988). https://doi.org/10.1063/1.454520
16. He, X., Zou, Q.: Analysis and boundary condition of the lattice Boltzmann BGK model with two velocity components (1995). https://doi.org/10.48550/ARXIV.COMP-GAS/9507002
17. Hohenberg, P.C., Halperin, B.I.: Theory of dynamic critical phenomena. Reviews of Modern Physics **49**(3), 435–479 (1977). https://doi.org/10.1103/RevModPhys.49.435
18. Kendon, V.M., Cates, M.E., Pagonabarraga, I., Desplat, J.C., Bladon, P.: Inertial effects in three-dimensional spinodal decomposition of a symmetric binary fluid mixture: a lattice boltzmann study. Journal of Fluid Mechanics **440**, 147–203 (2001). https://doi.org/10.1017/S0022112001004682
19. Krüger, T., Kusumaatmaja, H., Kuzmin, A., Shardt, O., Silva, G., Viggen, E.M.: The Lattice Boltzmann Method: Principles and Practice. Graduate Texts in Physics, Springer International Publishing, Cham (2017)
20. Kusumaatmaja, H., Yeomans, J.M.: Lattice Boltzmann Simulations of Wetting and Drop Dynamics. In: Kroc, J., Sloot, P.M., Hoekstra, A.G. (eds.) Simulating Complex Systems by Cellular Automata, pp. 241–274. Springer, Berlin, Heidelberg (2010). https://doi.org/10.1007/978-3-642-12203-3_11, https://doi.org/10.1007/978-3-642-12203-3_11
21. Laradji, M., Toxvaerd, S., Mouritsen, O.G.: Molecular Dynamics Simulation of Spinodal Decomposition in Three-Dimensional Binary Fluids. Physical Review Letters **77**(11), 2253–2256 (1996). https://doi.org/10.1103/PhysRevLett.77.2253
22. Moreno, R., Borga, M., Smedby, Ö.: Generalizing the mean intercept length tensor for gray-level images: Generalizing the mean intercept length tensor. Medical Physics **39**(7Part2), 4599–4612 (Jul 2012). https://doi.org/10.1118/1.4730502
23. Mudassir, M.A., Aslam, H.Z., Ansari, T.M., Zhang, H., Hussain, I.: Fundamentals and Design-Led Synthesis of Emulsion-Templated Porous Materials for Environmental Applications. Advanced Science **8**(22), 2102540 (2021). https://doi.org/10.1002/advs.202102540
24. Nonaka, A., Sun, Y., Bell, J., Donev, A.: Low Mach number fluctuating hydrodynamics of binary liquid mixtures. Communications in Applied Mathematics and

ICCS Camera Ready Version 2026
To cite this paper please use the final published version:
DOI: 10.1007/978-3-032-29909-3_45

Computational Science **10**(2), 163–204 (2015). https://doi.org/10.2140/camcos.2015.10.163
25. Pooley, C.M., Furtado, K.: Eliminating spurious velocities in the free-energy lattice Boltzmann method. Physical Review E **77**(4), 046702 (Apr 2008). https://doi.org/10.1103/PhysRevE.77.046702
26. Rothman, D.H., Keller, J.M.: Immiscible cellular-automaton fluids. Journal of Statistical Physics **52**(3–4), 1119–1127 (1988). https://doi.org/10.1007/BF01019743
27. Sander, E., Wanner, T.: Monte Carlo Simulations for Spinodal Decomposition. Journal of Statistical Physics **95**(5–6), 925–948 (1999). https://doi.org/10.1023/A:1004550416829
28. Semprebon, C., Krüger, T., Kusumaatmaja, H.: Ternary free-energy lattice Boltzmann model with tunable surface tensions and contact angles. Physical Review E **93**(3), 033305 (Mar 2016). https://doi.org/10.1103/PhysRevE.93.033305
29. Shan, X., Chen, H.: Lattice Boltzmann model for simulating flows with multiple phases and components. Physical Review E **47**(3), 1815–1819 (1993). https://doi.org/10.1103/PhysRevE.47.1815
30. Shan, X., Chen, H.: Simulation of nonideal gases and liquid-gas phase transitions by the lattice Boltzmann equation. Physical Review E **49**(4), 2941–2948 (1994). https://doi.org/10.1103/PhysRevE.49.2941
31. Shek, A.C.M., Kusumaatmaja, H.: Spontaneous phase separation of ternary fluid mixtures. Soft Matter **18**(31), 5807–5814 (2022). https://doi.org/10.1039/D2SM00413E
32. Shiohara, A., Prieto-Simon, B., Voelcker, N.H.: Porous polymeric membranes: Fabrication techniques and biomedical applications. Journal of Materials Chemistry B **9**(9), 2129–2154 (2021). https://doi.org/10.1039/D0TB01727B
33. Smit, Schneider, Odgaard: Star length distribution: A volume-based concept for the characterization of structural anisotropy. Journal of Microscopy **191**(3), 249–257 (1998). https://doi.org/10.1046/j.1365-2818.1998.00394.x
34. Soddemann, T., Dünweg, B., Kremer, K.: Dissipative particle dynamics: A useful thermostat for equilibrium and nonequilibrium molecular dynamics simulations. Physical Review E **68**(4), 046702 (2003). https://doi.org/10.1103/PhysRevE.68.046702
35. Swift, M.R., Orlandini, E., Osborn, W.R., Yeomans, J.M.: Lattice Boltzmann simulations of liquid-gas and binary fluid systems. Physical Review E **54**(5), 5041–5052 (1996). https://doi.org/10.1103/PhysRevE.54.5041
36. Swift, M.R., Osborn, W.R., Yeomans, J.M.: Lattice Boltzmann Simulation of Nonideal Fluids. Physical Review Letters **75**(5), 830–833 (1995). https://doi.org/10.1103/PhysRevLett.75.830
37. Travasso, R.D.M., Buxton, G.A., Kuksenok, O., Good, K., Balazs, A.C.: Modeling the morphology and mechanical properties of sheared ternary mixtures. The Journal of Chemical Physics **122**(19), 194906 (2005). https://doi.org/10.1063/1.1903883
38. Wagner, A.J., Yeomans, J.M.: Phase separation under shear in two-dimensional binary fluids. Physical Review E **59**(4), 4366–4373 (1999). https://doi.org/10.1103/PhysRevE.59.4366
39. Wang, F., Altschuh, P., Ratke, L., Zhang, H., Selzer, M., Nestler, B.: Progress Report on Phase Separation in Polymer Solutions. Advanced Materials **31**(26), 1806733 (2019). https://doi.org/10.1002/adma.201806733
40. Zou, X., Zhu, G.: Microporous Organic Materials for Membrane-Based Gas Separation. Advanced Materials **30**(3), 1700750 (2018). https://doi.org/10.1002/adma.201700750

ICCS Camera Ready Version 2026
To cite this paper please use the final published version:
DOI: 10.1007/978-3-032-29909-3_45